Supporting Information for

Mechanism of assembly of the dimanganese-tyrosyl radical cofactor of class Ib ribonucleotide reductase: Enzymatic generation of superoxide is required for tyrosine oxidation via a Mn(III)Mn(IV) intermediate

Joseph A. Cotruvo, Jr., [†,‡] *Troy A. Stich,* [§] *R. David Britt,** [§] *and JoAnne Stubbe** [†,&]

Department of Chemistry[‡] and Department of Biology[&], Massachusetts Institute of Technology, 77 Massachusetts Avenue, Cambridge, MA 02139

[§]Department of Chemistry, University of California, Davis, One Shields Avenue, Davis, California 95616

[*] To whom correspondence should be addressed. E-mail: stubbe@mit.edu, rdbritt@ucdavis.edu.

[†] Department of Chemistry, Massachusetts Institute of Technology.

[‡] Current address: Department of Chemistry, University of California, Berkeley, California 94720

[§] Department of Chemistry, University of California, Davis.

[&] Department of Biology, Massachusetts Institute of Technology.

SUPPORTING INFORMATION TABLE OF CONTENTS

S1. SUPPLEMENTARY EXPERIMENTAL SECTION

S1.1. Analysis of fluorometric data to determine the affinity of the $NrdI_{hq}$•Mn^{II}_2-NrdF interaction

At each point in the titration of 1 μM Mn^{II}-loaded apoNrdF with $NrdI_{hq}$, the fluorescence change associated with binding of $NrdI_{hq}$ to NrdF, ΔF, was calculated according to

$$\Delta F = F - F_0 - \mathbf{F_L}[L]_T \quad \text{(S1)}$$

where F is the total fluorescence at 517 nm, F_0 is the initial fluorescence at 517 nm of the solution containing 1 μM Mn^{II}_2-NrdF, $\mathbf{F_L}$ is the molar fluorescence of unbound $NrdI_{hq}$ (see below), and $[L]_T$ is the total concentration of NrdI (μM) at each point in the titration. The concentration of unbound $NrdI_{hq}$, [L], was extracted after each addition of $NrdI_{hq}$ by rearranging equation (S2) to give equation (S3):

$$F = \mathbf{F_L}[L] + \mathbf{F_{ML}}([L]_T - [L]) \quad \text{(S2)}$$

$$[L] = \frac{F - \mathbf{F_{ML}}[L]_T}{\mathbf{F_L} - \mathbf{F_{ML}}} \quad \text{(S3)}$$

where $\mathbf{F_{ML}}$ is the molar fluorescence of bound $NrdI_{hq}$.

$\mathbf{F_L}$ was determined by addition in 1 or 2 μL aliquots of a solution containing $NrdI_{hq}$ (240 μM) and dithionite (100 μM) in Buffer B into 700 μL Buffer B containing 100 μM dithionite (final concentration of $NrdI_{hq}$ in the cuvette was 15 μM). Fluorescence at 517 nm (after accounting for the volume change upon NrdI addition) was plotted against $NrdI_{hq}$ added and the slope of the least-squares regression line represented $\mathbf{F_L}$.

$\mathbf{F_{ML}}$ was determined relative to $\mathbf{F_L}$ by acquiring spectra of 700 μL solutions of 2 μM $NrdI_{hq}$ and 100 μM dithionite in Buffer B, in the presence of various concentrations of Mn^{II}-loaded NrdF from 0 to 25 μM. The fluorescence intensity was saturated at ~15 μM NrdF, and this value was used to determine $\mathbf{F_{ML}} = 2.4\mathbf{F_L}$.

For each point in the Mn^{II}-loaded NrdF/$NrdI_{hq}$ titration, the values of ΔF and [L] were plotted and fit to eq. S4,[1]

$$\Delta F = (nK[L]\Delta F_{max})/(1 + K[L]) \quad \text{(S4)}$$

where K is the association constant for NrdI-NrdF, n is the stoichiometry of NrdI binding (per NrdF dimer), and ΔF_{max} is the maximum fluorescence change associated with $NrdI_{hq}$ binding, expressed as

$$\Delta F_{max} = [M]_T(\mathbf{F_{ML}} - \mathbf{F_L}) \quad \text{(S5)}$$

where $[M]_T$ is the concentration of NrdF.

S1.2. Determination of the UV-visible absorption spectra of the Mn^{III}_2 cluster and the Y•

S1.2.1. Reduction of Y• using hydroxylamine. Mn^{III}_2-Y• was prepared as described in section 2.5.1. At 23 °C, a UV-vis spectrum of Mn^{III}_2-Y• NrdF (200 μM, 300 μL) was acquired in Buffer B containing 5 mM EDTA. The EDTA was present to remove Mn^{II} formed by reduction of Mn^{III}_2 cluster by NH_2OH. After addition of NH_2OH to a final concentration of 0.5 mM, spectra were acquired every 1-2 min, until the sharp signature of the Y• at 410 nm was completely abolished (<10 min). The sample was immediately loaded at 4 °C onto a Sephadex G-25 column (1 × 6.5 cm, 5 mL) preequilibrated and eluted with 50 mM HEPES, 5% glycerol, pH 7.6 (Buffer B), and 0.5 mL fractions were collected. Protein-containing fractions were pooled and concentrated to 300 μL using a Microcon 30 kDa MWCO centrifugal filtration device (Amicon). A UV-vis spectrum was acquired of the resulting undiluted Mn^{III}_2-NrdF, the protein concentration was measured (ε_{280} = 110 mM^{-1} cm^{-1})[2] and Mn was quantified by AA spectroscopy.

S1.2.2. Mn^{III}_2 cluster extinction coefficient determination. Because the extinction coefficients of Mn^{III}_2 clusters are very low, the contribution of the protein scattering was

subtracted from the Mn^{III}_2-NrdF spectrum using a spectrum of apoNrdF. Using the resulting spectrum and the AA results, the extinction coefficient for the Mn^{III}_2 cluster was determined assuming all of the Mn associated with NrdF was in Mn^{III}_2 clusters. While we cannot demonstrate the validity of this assumption with certainty, 70% of the Mn is associated with Y• in the initial Mn^{III}_2-Y• NrdF and is therefore dinuclear. Furthermore, even if the remaining 30% of Mn is mononuclear, the spectrum of two mononuclear Mn^{III} ions should resemble that of the Mn^{III}_2 cluster, as Mn^{III}_2 cluster absorption bands likely arise from *d-d* rather than charge transfer transitions.[3]

S1.2.3. Y• spectrum determination. As each Y• is associated with 2 Mn^{III} ions, the initial 200 μM Mn^{III}_2-Y• NrdF sample (1.0 Mn/β2, 0.36 Y•/β2) contained ~30 μM Mn^{III}_2 cluster not associated with Y•. Subtraction of the protein scattering and the contribution of 30 μM Mn^{III}_2 cluster from the initial NrdF spectrum yielded the spectrum of the Mn^{III}_2-Y• cofactor. However, subtracting the remaining amount of Mn^{III}_2 cluster (70 μM, associated with Y•) from the Mn^{III}_2-Y• cofactor spectrum yielded a Y• spectrum with negative absorbances. Therefore, the Mn^{III}_2 cluster spectrum was scaled by 0.35 and subtracted from the Mn^{III}_2-Y• cofactor spectrum; this scaling factor was determined to be the value that resulted in a Y• spectrum similar to that of previously characterized diferric-Y• cofactors, with a sharp feature at ~410 nm, a shoulder at ~390 nm, and a broad, low intensity band from 500 to 700 nm.[4] This difference spectrum represents the Y•. The extinction coefficient of Y• was calculated using this spectrum and the Y• concentration of the initial sample determined by EPR spectroscopy. The entire determination was repeated 5 times using two different preparations of Mn^{III}_2-Y• NrdF and the average was used for Figure 1B.

S1.3. Construction, expression, and purification of Y105F NrdF. The primers for site-directed mutagenesis were 5'-C GCT GTC CAT GCG AAG TCG TTC TCT AAT ATT TTC ATG-3' (mutated codon underlined) and its reverse complement, obtained from Invitrogen. Mutagenesis of pET14b-*nrdF*[5] was carried out using Platinum Pfx DNA polymerase (Invitrogen) following the manufacturer's protocol. Clones were sequenced at the MIT Biopolymers Facility. Y105F-NrdF was expressed in *E. coli* as apoprotein and purified similarly to wt apoNrdF.[5] Briefly, *E. coli* BL21(DE3) cells transformed with pET14b-*nrdF*(Y105F) were grown in LB to an OD_{600} of 0.6, at which point 100 μM 1,10-phenanthroline was added to the culture medium. After 25 min, protein expression was induced by addition of 0.4 mM IPTG. Cells were grown for an additional 4 h and harvested by centrifugation, yielding 14 g wet cell paste from 8 L culture.

The cell paste was resuspended in 70 mL of 50 mM sodium phosphate, 10 mM imidazole, 5% glycerol, pH 7.0, with 100 μM 1,10-phenanthroline, 1 mM PMSF, and 5 U/mL DNase (Roche). After lysis by passage through a French pressure cell (14000 psi) and centrifugation (35000 *g*, 20 min), the supernatant (75 mL) was loaded to a 4 mL Ni-NTA column, which was washed with 35 column volumes of the same buffer. The protein was eluted with 7 column volumes of 50 mM sodium phosphate, 250 mM imidazole, 5% glycerol, pH 7.0, and exchanged into 50 mM HEPES, 5% glycerol, pH 7.6 by repeated concentration and dilution steps using an Amicon Ultra 30 kDa MWCO centrifugal filtration device. The yield of apo-Y105F-NrdF was 95 mg (7 mg/g cell paste).

S1.4. Attempts to assemble Mn^{III}_2-Y• cofactor using exogenous superoxide

The experimental setup was similar to that of Bull and Fee.[6] Stable solutions of superoxide were prepared as described by Valentine and Curtis,[7] under Ar on the day of the SF

experiment. In a crimp vial, 0.4 g 18-crown-6 and ~60 mg KO_2 (greater than the solubility limit) were weighed out, and 5 mL anhydrous DMSO was added using a gastight syringe. The solution was mixed and the vial was sealed. The SF apparatus, maintained at 25 ± 1 °C using a circulating water bath, was set up according to the scheme below:

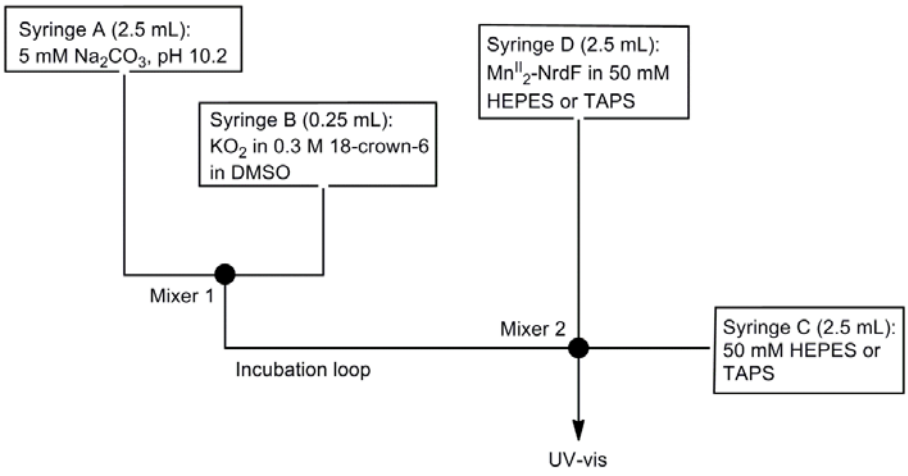

Syringes C and D contained either 50 mM HEPES, pH 7.6; 50 mM HEPES, pH 8.0; or 50 mM TAPS, pH 8.5. These buffers were sparged with Ar for 10 min before loading onto the SF instrument. In experiments containing NrdF, syringe D also contained 40 μM apoNrdF and 160 μM $MnCl_2$. The contents of syringes A and B were mixed (drive volume 200 μL) and, after aging for 10 ms, mixed with the contents of syringes C and D (drive volume 180 μL). The initial concentration of superoxide, generally >1 mM, was assessed from the A_{300nm} after the second mix, using $\varepsilon_{300} = 284\ M^{-1}\ cm^{-1}$.[6] The presence of Mn^{II}-loaded NrdF did not significantly affect the rate of disappearance of superoxide (monitored at 300 nm) and did not significantly affect the SF traces at 340 nm, suggesting no evidence of cluster assembly under these conditions.

S2. SUPPLEMENTARY RESULTS

S2.1. $NrdI_{sq}$ is fully in the neutral form at pH 7.6. It is important to establish the protonation state of NrdI's FMN cofactor in the semiquinone (sq) form, as flavoproteins can exhibit either neutral (FMNH•) and anionic ($FMN^{\bullet -}$) sq forms. These protonation states can be distinguished on the basis of their UV-vis absorption[8] and EPR[9] spectra. The visible absorption in the 500-600 nm region (Figure 1A) and a peak-to-trough linewidth of 1.9 mT in the EPR spectrum of $NrdI_{sq}$ (Figure S1) indicate formation of neutral sq in NrdI. To further support these findings, $NrdI_{hq}$ was reacted with O_2 at pHs 7.6, 7.0, and 6.5, monitored by SF absorption spectroscopy (Table S1). Oxidation of $NrdI_{hq}$ to the anionic sq, or oxidation of neutral $NrdI_{sq}$ to $NrdI_{ox}$, would be accompanied by loss of a proton from the flavin cofactor. Therefore, whether the rate constant for sq formation or decay is pH dependent would reveal the protonation state of the $NrdI_{sq}$ if the proton loss precedes or is involved in the rate determining step. As noted in Table S1, the apparent rate constant for sq formation is independent of pH, whereas the rate constant for sq decay decreases with decreasing pH. These results together suggest that only conversion of $NrdI_{sq}$ to $NrdI_{ox}$ is associated with loss of a proton, putatively from the FMN cofactor itself; i.e. $NrdI_{sq}$ is in the FMNH• form.

A possible source of the two phases for $NrdI_{hq}$ oxidation observed at pH 7.6 in the presence of NrdF (Tables 1 and 2, main text) was that, in addition to neutral sq, small amounts of anionic sq could have been present. To establish the absence of anionic sq contributing to the second phase, NrdI was exchanged into 50 mM sodium phosphate, 5% glycerol, pH 6.5 and 50 mM TAPS, 5% glycerol, pH 9.0, degassed, and ~100 μM NrdI was titrated anaerobically with 0.5 equiv dithionite. These samples were loaded anaerobically into EPR tubes and frozen in isopentane (-140 °C). The EPR spectra were collected at 77 K (Figure S1). The EPR spectra of

$NrdI_{sq}$ at pH 6.5 – 9.0 are indistinguishable, with a peak-to-trough linewidth of 1.9 mT. There is also no appreciable difference in the EPR spectra in the presence of NrdF or during cluster assembly reactions (Figure S1, green). By contrast, anionic sqs exhibit a peak-to-trough distance of 1.5 mT. These results support the conclusion that $NrdI_{sq}$ is fully in the neutral form in all of our experiments, and the second phase for $NrdI_{hq}$ oxidation is not associated with anionic sq chemistry.

S2.2. Magnetic parameters for simulation of the Y• EPR spectrum

The Y• EPR spectrum was simulated using $S = 1/2$ and $g = [2.0085\ 2.0045\ 2.0022]$. The Gaussian linewidth (FWHM) was 0.4 mT and the Lorentzian linewidth (FWHM) was 0.8 mT. The calculated proton hyperfine interactions are shown below in MHz (couplings computed using $\Theta = 44°$):

	A_x	A_y	A_z
β-H1	25.4	25.4	32.5
β-H2	1.0	1.0	10.4
H3	-25.2	-14.0	-22.4
H5	-25.2	-14.0	-22.4

The HFI for H3 and H5 were fixed at values that are typical for tyrosine radicals in class Ib RNRs ($A(^1$H3/5) = [−25.2 −14.0 −22.4] MHz).[10] The McConnell relations were used to calculate the hyperfine tensors for the two β-protons. The isotropic part of the HFI (A_{iso}) is computed according to eq. S6:

$$A_{iso} = B \cdot \rho C1 \cdot \cos^2 \Theta \qquad \text{(S6)}$$

The unpaired spin density in the $2p_z$ orbital of carbon 1 (ρC1) was set to 0.342, a value determined from density functional theory.[11] The McConnell constant B was set to the literature value of 162 MHz.[12] The angle Θ describes the dihedral angle from the plane normal of the

phenyl ring to the β-proton. The anisotropic part of the β-proton HFI was calculated using the relation (eq. S7):

$$A_{||}/A_{\perp} = a + b * e^{c\theta} \quad \text{(S7)}$$

with a = 1.12, b = 9.37e^{-6}, and c = 0.162 °$^{-1}$.[13]

The high-temperature (100 K) spectrum of the fully assembled cofactor (Figure S6, blue trace) was best fit with Θ = 44°. Additional simulations are provided using the dihedral angles of 25 and 32° determined from the x-ray crystallographic structure of each subunit of the reduced form of NrdF.[14] As can be seen in Figure S6, these other values of Θ do not reproduce the prominent spectral feature at 333.6 mT (vertical black line).

S2.3. Reaction of $NrdI_{hq}$ with O_2 monitored by SF absorption

This section describes in detail how it was established that $NrdI_{hq}$ reacts with O_2 primarily to produce $O_2^{\bullet-}$, like typical flavodoxins.[15]

Scheme S1. Two pathways for reaction of $NrdI_{hq}$ with O_2 to produce $O_2^{\bullet-}$ and H_2O_2. The bracket around the C4a-hydroperoxide indicates that it was not observed in our studies.

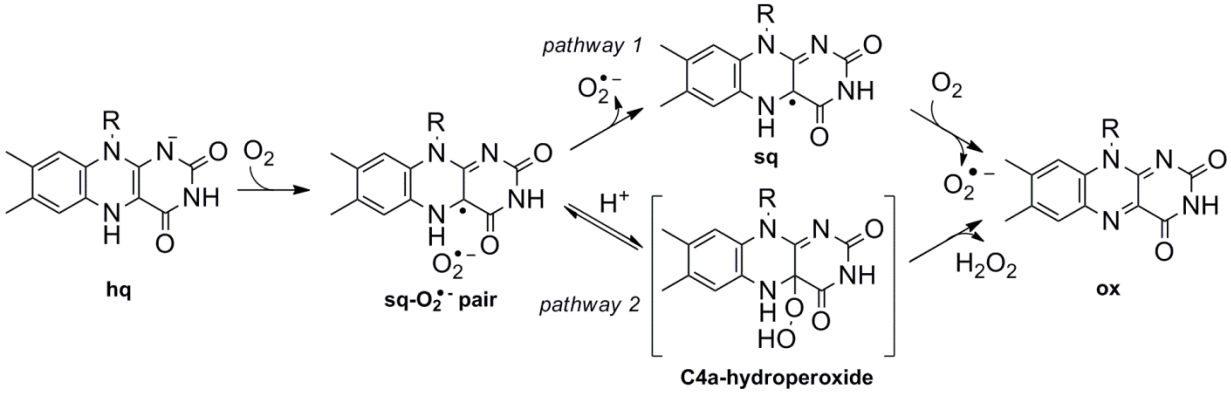

S2.3.1. Background: reaction of flavodoxins with O_2. The chemistry of reduced flavoproteins with O_2 is complex and can follow multiple pathways;[16] however, the common first step is believed to be a single electron transfer to O_2 to produce a caged sq-$O_2^{\bullet-}$ radical pair.[17,18]

In flavodoxins[15,19] and oxidases,[20] respectively, this species partitions between pathways 1 and 2 (Scheme S1), respectively, liberating $O_2^{\bullet-}$ in the former case and H_2O_2 in the latter. The intermediacy of the radical pair has been deduced from model studies;[17,18] supporting evidence has recently been provided by studies of glycolate oxidase.[21]

To our knowledge, the reaction of a flavodoxin with O_2 has only been investigated in detail in a thesis by Ballou.[19] In the *Peptostreptococcus elsdenii* flavodoxin, Ballou observed that the SF data could be fit by the model described by eq. 1 and 2 (from main text and reproduced below) when SOD was included in the reaction.[22] The SOD was proposed to prevent reaction of the $O_2^{\bullet-}$ produced by eq. 1 and 2 with the hq (E-FMNH$^-$) and sq (E-FMNH•) forms (eq. S8 and S9). Our investigations of the reaction of $NrdI_{hq}$ with O_2 indicated that SOD's effect on the reaction kinetics was similar to that in *P. elsdenii* flavodoxin (Figure S8A), demonstrating that $O_2^{\bullet-}$ is a product of the reaction. Thus, to decrease the potential complexity that could arise from the reactions shown in eq. S8 and S9, the experiments described subsequently contained SOD. Studies indicated that 50 U/mL SOD (concentration after mixing) was sufficient to suppress these reactions, although in some experiments 250 U/mL SOD was used.

$$\text{E-FMNH}^- + O_2 \xrightarrow{k_1} \text{E-FMNH}^\bullet + O_2^{\bullet-} \quad (1)$$

$$\text{E-FMNH}^\bullet + O_2 \xrightarrow{k_2} \text{E-FMN} + O_2^{\bullet-} \quad (2)$$

$$\text{E-FMNH}^- + O_2 \xrightarrow[H^+]{k_3} \text{E-FMN} + H_2O_2 \quad (3)$$

$$\text{E-FMNH}^- + \text{E-FMN} \underset{k_{-4}}{\overset{k_{+4}}{\rightleftharpoons}} 2\ \text{E-FMNH}^\bullet \quad (4)$$

$$\text{E-FMNH}^- + O_2^{\bullet-} \xrightarrow[H^+]{k_5} \text{E-FMNH}^\bullet + H_2O_2 \quad (S8)$$

$$\text{E-FMNH}^\bullet + O_2^{\bullet-} \xrightarrow[H^+]{k_6} \text{E-FMN} + H_2O_2 \quad (S9)$$

S2.3.2. Reaction of $NrdI_{hq}$ with O_2, monitored by SF absorption. We initially investigated the reaction of 20 μM $NrdI_{hq}$, in one syringe, with O_2-saturated buffer containing 500 U/mL SOD, in a second syringe, mixed in a 1:1 ratio at 25 °C. The reaction was monitored from 310 to 700 nm at 10 nm increments (Figure S9A). Singular value decomposition (SVD) of the data indicated significant contribution from three absorbing species: $NrdI_{hq}$, $NrdI_{sq}$, and $NrdI_{ox}$, suggestive that a flavin C4a-hydroperoxide intermediate[23] (Scheme S1) is not observed. The data were fit globally using KinTek Explorer with SpectraFit to a model consisting of eq. 1, 2, and 4 (Scheme S1, pathway 1), and the spectra of these species were extracted (Figure S9B). The rate constants k_{+4} and k_{-4} were fixed at the values determined in the subsequent section, S2.4 (Table S2). The extracted $NrdI_{sq}$ spectrum differed from that in Figure 1A (main text), however, suggesting that it contained a contribution from $NrdI_{ox}$. Thus, an additional pathway for $NrdI_{ox}$ formation was considered (Scheme S1, pathway 2). As no evidence for a flavin hydroperoxide is observed, the elimination of H_2O_2 in Scheme S1, pathway 2, must be very fast, allowing us to simplify this pathway to eq. 3. The new kinetic model thus initially included reactions 1-4. However, removal of eq. 4 did not significantly affect the fits and was thus discarded. This model gave k_1 = 1.6 ± 0.1 mM^{-1} s^{-1}, k_2 = 2.0 ± 0.1 mM^{-1} s^{-1}, and k_3 = 0.7 ± 0.1 mM^{-1} s^{-1}, and reproduced the spectrum of $NrdI_{sq}$ (Figure S9D). Based on this model, we tentatively conclude that, in the absence of NrdF, $NrdI_{hq}$ reacts with O_2 by two predominant pathways to form 1) $NrdI_{sq}$ and $O_2^{\bullet-}$ and 2) $NrdI_{ox}$ and H_2O_2. Given the relative values of k_1 and k_3, ~70% of $NrdI_{hq}$ reacts by the former pathway to produce $O_2^{\bullet-}$ and 30% to produce H_2O_2.

S2.4. Determination of the rate constants for NrdI disproportionation and comproportionation and their dependence on NrdF. In other flavodoxins, E-FMN and E-$FMNH^-$ can comproportionate (eq. 4).[15] It is thus important to assess if this reaction interferes

with the kinetics of $NrdI_{hq}$-mediated oxidant delivery to NrdF. The values of k_{+4} and k_{-4} were assessed for NrdI at pH 7.6 and 25 °C by mixing anaerobic solutions of 20 μM $NrdI_{hq}$ and $NrdI_{ox}$ and monitoring change in A_{610nm}, associated with sq formation (Figure 1A), using SF spectroscopy (Figure S11A).[24] Similar experiments were also carried out in the presence of sufficient concentrations of apo-NrdF to form ~98% complex with NrdI (Figure S11B). The SF traces were fit to the model in eq. 4 using KinTek Explorer (Table S2). Both k_{+4} and k_{-4} are decreased 20-fold when $NrdI_{hq}$ is complexed to NrdF. This result is consistent with the burial of the dimethylbenzene moiety of NrdI's FMN cofactor in NrdF, observed in the crystal structure of the *E. coli* NrdI•NrdF complex.[25] This moiety has been suggested to be involved in electron transfer in flavodoxins.[26] The ratio k_{+4}/k_{-4} is 0.5, implying 33% sq stabilization, similar to the K_{eq} calculated from equilibrium titrations with dithionite (0.7, 30% sq stabilized). k_{+4} and k_{-4} in the presence of NrdF are sufficiently small that they do not contribute significantly to the reaction of $NrdI_{hq}$•NrdF with O_2, given the measured rate constants in section 3.6 (main text).

S2.5. Magnetic parameters for simulation of the $Mn^{III}Mn^{IV}$ EPR spectrum

The following parameters were used to simulate the $Mn^{III}Mn^{IV}$ EPR spectrum: $S = 1/2$, g = [2.008 2.008 1.98], and a Gaussian linewidth of 1.4 mT (FWHM). The ^{55}Mn hyperfine interaction was simulated (all values in MHz) using A(Mn1) = [-465 -435 -310] MHz and A(Mn2) = [230 230 240] MHz.

S2.6. Attempt to characterize the $Mn^{III}Mn^{IV}$ intermediate using Y105F NrdF. Studies of Fe^{III}_2-Y• cofactor assembly in class Ia RNRs have shown that mutation of the radical-harboring tyrosine residue to phenylalanine increases the lifetime of intermediate **X**.[27-29] *B. subtilis* Y105F-NrdF was expressed and purified as the apoprotein (Figure S17A). To examine metal binding,

the protein was loaded with 3.5 Mn^{II}/β2 and analyzed by EPR spectroscopy; the spectrum (Figure S17B) exhibits little evidence of mononuclear Mn^{II}, in contrast to wt NrdF (Figure 2A), suggesting tighter Mn^{II} binding to Y105F than to wt NrdF. Fluorescence titrations (Figure S18) indicated that, although $NrdI_{hq}$ bound to Mn^{II}_2-Y105F-NrdF, it bound either incorrectly or much more weakly than to wt NrdF. Consistent with this result, no evidence of $Mn^{III}Mn^{IV}$ intermediate formation was observed in SF studies monitoring reaction of $NrdI_{hq}$ with O_2 in the presence of Mn^{II}_2-Y105F-NrdF carried out under conditions similar to those with wt NrdF (Figure S19). Together, the data suggest that $Mn^{III}Mn^{IV}$ is not formed in the Y105F mutant because $NrdI_{hq}$ does not bind well or correctly to it (see section 4.3 and Figure S20 for a possible explanation).

S2.7. Cofactor assembly using exogenous $O_2^{\bullet-}$? Our identification of $O_2^{\bullet-}$ produced by NrdI as the oxidant required for Mn^{III}_2-Y• cofactor generation led us to investigate whether exogenous $O_2^{\bullet-}$ could mediate cluster assembly as well. We previously attempted to activate *E. coli* Mn^{II}_2-NrdF using $O_2^{\bullet-}$ produced catalytically by the xanthine/xanthine oxidase system, without success.[30] To test whether higher $O_2^{\bullet-}$ concentrations would allow for cofactor assembly in *B. subtilis* NrdF, a stable solution of potassium superoxide was prepared in a solution of 18-crown-6 in anhydrous DMSO.[7] This solution was mixed in the sequential mixing SF apparatus described in section S1.3, first with pH 10.2 buffer, and then with Mn^{II}_2-loaded NrdF at pH 7.6-8.5.[6] A similar method is routinely used to monitor activity of SODs.[6] Despite the presence of >1 mM $O_2^{\bullet-}$ and 20 μM Mn^{II}-loaded NrdF immediately after mixing, no evidence of $Mn^{III}Mn^{IV}$ formation was observed at 340 nm, nor was there any apparent effect of the presence of NrdF on the rate of disappearance of $O_2^{\bullet-}$ monitored at 300 nm. One explanation for this result is that, under these experimental conditions, the reaction of the Mn^{II}_2 center in NrdF with $O_2^{\bullet-}$ may not

be able to compete kinetically with the disproportionation of $O_2^{\bullet-}$ in solution ($k_{obs} \sim 10^5$ M^{-1} s^{-1} at pH 8, 23 °C),[31] even in the presence of large excesses of $O_2^{\bullet-}$. Alternatively, the presence of NrdI may be required to funnel $O_2^{\bullet-}$ into the metal site; $NrdI_{hq}$ or $NrdI_{sq}$ could not be included in this experiment because they would react with $O_2^{\bullet-}$. These results further highlight the essential role of NrdI in Mn^{III}_2-Y• cofactor assembly.

S3. SUPPLEMENTARY TABLES AND FIGURES

Table S1. Apparent rate constants at 25 °C for reaction of $NrdI_{hq}$ with 0.6 mM O_2 in the presence of SOD, by SF UV-vis spectroscopy

pH	k (s^{-1}), sq formation	k (s^{-1}), sq decay
7.6[a]	1.6	1.1
7.0[b]	1.7	0.4
6.5[c]	1.7	0.2

[a] 1:1 mixing of 20 μM $NrdI_{hq}$ with O_2-saturated buffer, 100 U/mL SOD. Buffer: 50 mM HEPES, 5% glycerol, pH 7.6. See also Table 1.
[b] 1:1 mixing of 30 μM $NrdI_{hq}$ with O_2-saturated buffer, 100 U/mL SOD. Buffer: 50 mM sodium phosphate, 5% glycerol, pH 7.0
[c] 1:1 mixing of 30 μM $NrdI_{hq}$ with O_2-saturated buffer, 100 U/mL SOD. Buffer: 50 mM sodium phosphate, 5% glycerol, pH 6.5

Table S2. Rate constants (mM^{-1} s^{-1}) at 25 °C for NrdI comproportionation (k_{+4}) and disproportionation (k_{-4})

	NrdI alone	NrdI + apoNrdF[a]
k_{+4}	13 ± 4	0.6 ± 0.2
k_{-4}	25 ± 3	1.3 ± 0.1

[a] ~98% $NrdI_{hq}$ complexed according to section 3.4

Table S3. Apparent rate constants in the reaction of 100 μM $NrdI_{hq}$ and 150 μM Mn^{II}-loaded NrdF (3.5 Mn/β2) mixed 1:1 with O_2-saturated buffer, determined by fits to single-wavelength SF (610 nm) or RFQ-EPR (10 or 77 K) data (Figures 4 and 5).

Reaction	610 nm k (s^{-1})	ΔA	Amplitude (μM)	340 nm k (s^{-1})	ΔA	Amplitude (μM)	410 nm k (s^{-1})	ΔA	Amplitude (μM)	RFQ-EPR k (s^{-1})	Amplitude (μM)[a]
sq formation	40	0.18	37	40	0.15	30	48	-0.03	-- [b]	88 ± 38	34 ± 16
unknown phase	8	0.05	10								
sq decay	0.65	-0.24	49	0.22	-0.077	17	0.74	0.28[b]	66[b]	0.8 ± 0.2	27 ± 2
$Mn^{III}Mn^{IV}$ formation	NA[c]	NA	NA	2.5	0.17	13 ± 4 [d]	NA[c]	NA	NA	2.2 ± 0.4	19 ± 6[e]
$Mn^{III}Mn^{IV}$ decay / Y• formation	0.15	0.012	27 μM Mn^{III}_2-Y•[f]	0.08	-0.16	19 ± 6 μM $Mn^{III}Mn^{IV}$ [f]	0.09	0.054	25 ± 8 μM $Mn^{III}Mn^{IV}$ [f]	0.12 ± 0.02	22 ± 7[e]

[a] Adjusted for packing factor

[b] The difference in extinction coefficients of $NrdI_{hq}$ and $NrdI_{sq}$ at 410 nm is <0.4 mM^{-1} cm^{-1}; consequently, the small uncertainty in the estimated spectrum of $NrdI_{sq}$ makes this value not meaningful.

[c] NA: not applicable. At 610 nm, $Mn^{III}Mn^{IV}$ does not contribute significantly (Figure S14). At 410 nm, given that the $Mn^{III}Mn^{IV}$ intermediate should contribute ~+0.07 to ΔA_{410} (Figure S14), it is probable that this phase was not resolved from sq decay in the fits because its rate constant for formation is somewhat similar to that for sq decay, and of the same sign. If this is true, the amplitude of the "sq decay" component of this phase at this wavelength would become a more reasonable 50 μM.

[d] For phases involving $Mn^{III}Mn^{IV}$ formation or decay, we have assumed ε_{340} = 13 ± 4 mM^{-1} cm^{-1} and ε_{410} = 3 ± 1 mM^{-1} cm^{-1}. These values were determined from Figure S14 on the basis of the estimated UV-vis spectrum of the intermediate and the quantification of the EPR spectrum of $Mn^{III}Mn^{IV}$ by simulation at 3 timepoints (section 2.9).

[e] ND: not determined (simulation of EPR spectra is required for reliable extraction of concentrations)

[f] Concentrations of Mn^{III}_2-Y• (27 μM) and Mn^{III}_2 (11 μM) are taken as given (section 2.8.1).

Figure S1. $NrdI_{sq}$ is entirely in the neutral form at pH 7.6. NrdI (~100 μM) in 50 mM sodium phosphate (pH 6.5, red), HEPES (pH 7.6, black), or TAPS (pH 9.0, blue) buffers (all containing 5% glycerol) was titrated anaerobically with ~50 μM sodium dithionite and transferred anaerobically to EPR tubes, which were frozen in isopentane at -140 °C. In addition, a solution of 100 μM $NrdI_{hq}$ and 150 μM Mn^{II}-loaded NrdF (3.5 Mn^{II}/β2) was mixed 1:1 with O_2-saturated HEPES buffer, 25 °C, and the reaction was quenched at 48 ms in isopentane at -140 °C by the RFQ method (green). The samples were analyzed by X-band EPR spectroscopy at 77 K. Parameters: 9.45 GHz frequency, 5 μW power, 100 kHz modulation frequency, 0.15 mT modulation amplitude, 5.12 ms time constant, 5×10^4 receiver gain. The samples are shown after scaling for concentration. The peak-to-trough distance (1.9 mT) is indicated by dotted lines.

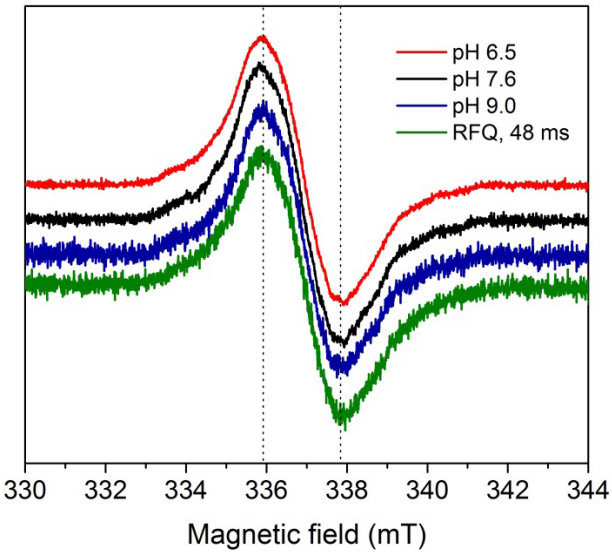

Figure S2. Reduction of Mn^{III}_2-Y• NrdF (200 μM) with hydroxylamine (0.5 mM), monitored by UV-vis absorption spectroscopy at 23 °C. (A) UV-vis spectrum was acquired of 300 μL Mn^{III}_2-Y• NrdF (200 μM) in Buffer B containing 5 mM EDTA (0 min, black). After addition of NH_2OH to a final concentration of 0.5 mM, spectra were acquired at the indicated times (1, 2.5, 4, 6, 8, and 10 min). By 10 min, the sharp feature of the Y• at 410 nm was completely abolished. The spectra show that Mn^{III}_2 cluster is also partially reduced during this treatment (see Figure 1B). (B) Comparison of the spectra taken before NH_2OH addition (0 min) and 1 min after show a significant, reproducible increase in absorption evident between 450 and 550 nm accompanying reduction of Y•. This increase supports the conclusion that reduction of Y• increases the extinction coefficient of the formerly associated Mn^{III}_2 cluster. Because reduction of Y• and Mn^{III}_2 cluster are occurring simultaneously (tending to decrease overall absorption), the effect of Y• reduction on increasing Mn^{III}_2 cluster extinction coefficient is underestimated by this spectrum.

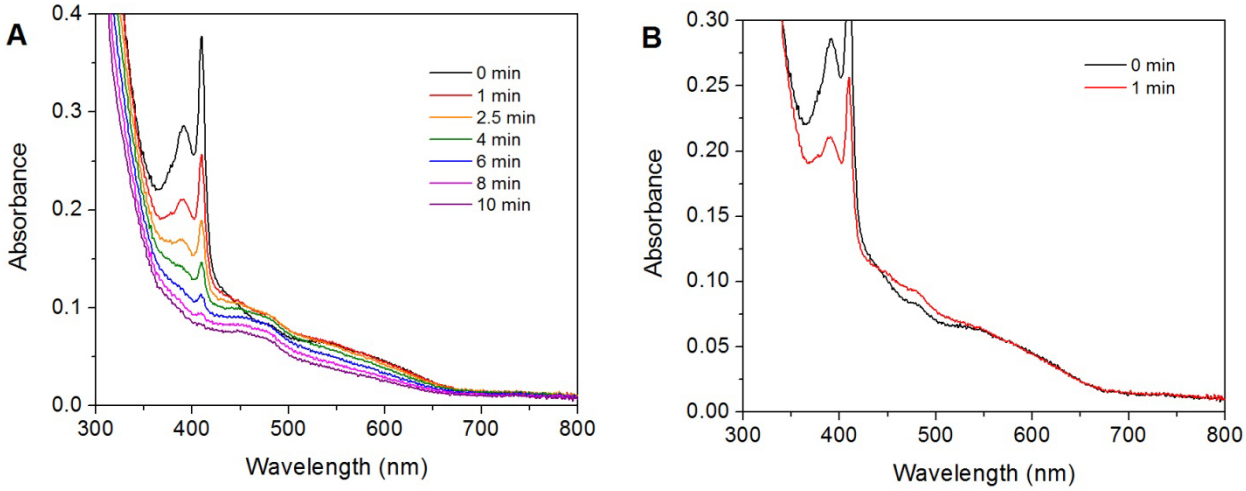

Figure S3. Titration of apoNrdF with Mn^{II}. (A) *B. subtilis* apoNrdF (75 μM) was incubated with 1.0, 1.5, 2.0, 2.5, 3.0, 3.5, and 4.0 Mn^{II}/β2. In the 10 K EPR spectra of the samples, unbound, mononuclear Mn^{II} (sextet centered at g = 2.0, 310-360 mT) is evident even in the 1.0 Mn/β2 sample. At 4.0 Mn^{II}/β2, ~20% of Mn^{II} is unbound, as revealed by analysis of the same sample at 293 K.

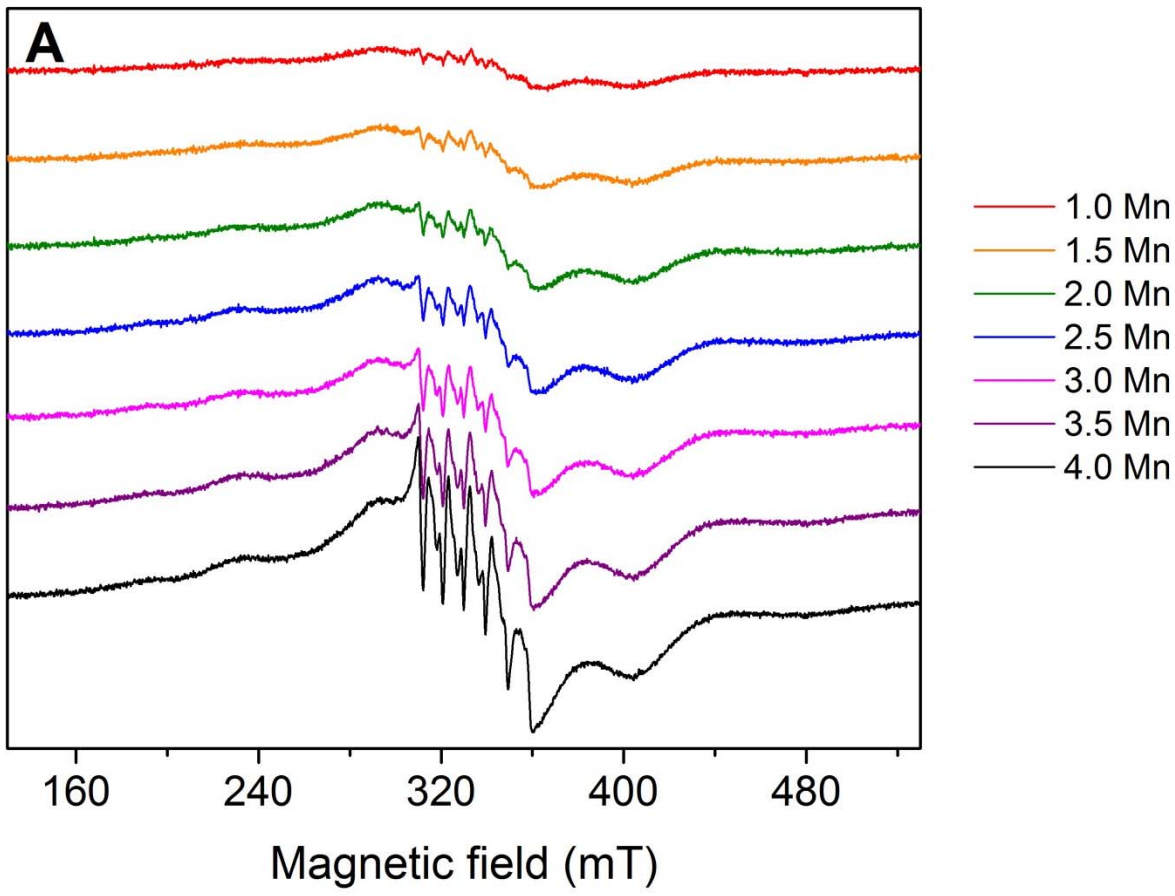

Figure S3, continued. B) An analogous titration of 30 μM *E. coli* apoNrdF with Mn^{II}. Unbound, mononuclear Mn^{II} is apparent only at 4.0 Mn/β2. The absence of mononuclear Mn^{II} even at low Mn^{II}/β2 also suggests highly cooperative Mn^{II} binding in this system. Acquisition parameters: 9.385 GHz, 0.1 mW power, 0.4 mT modulation amplitude, 100 kHz modulation frequency, 2.52×10^4 gain, 5.12 ms time constant.

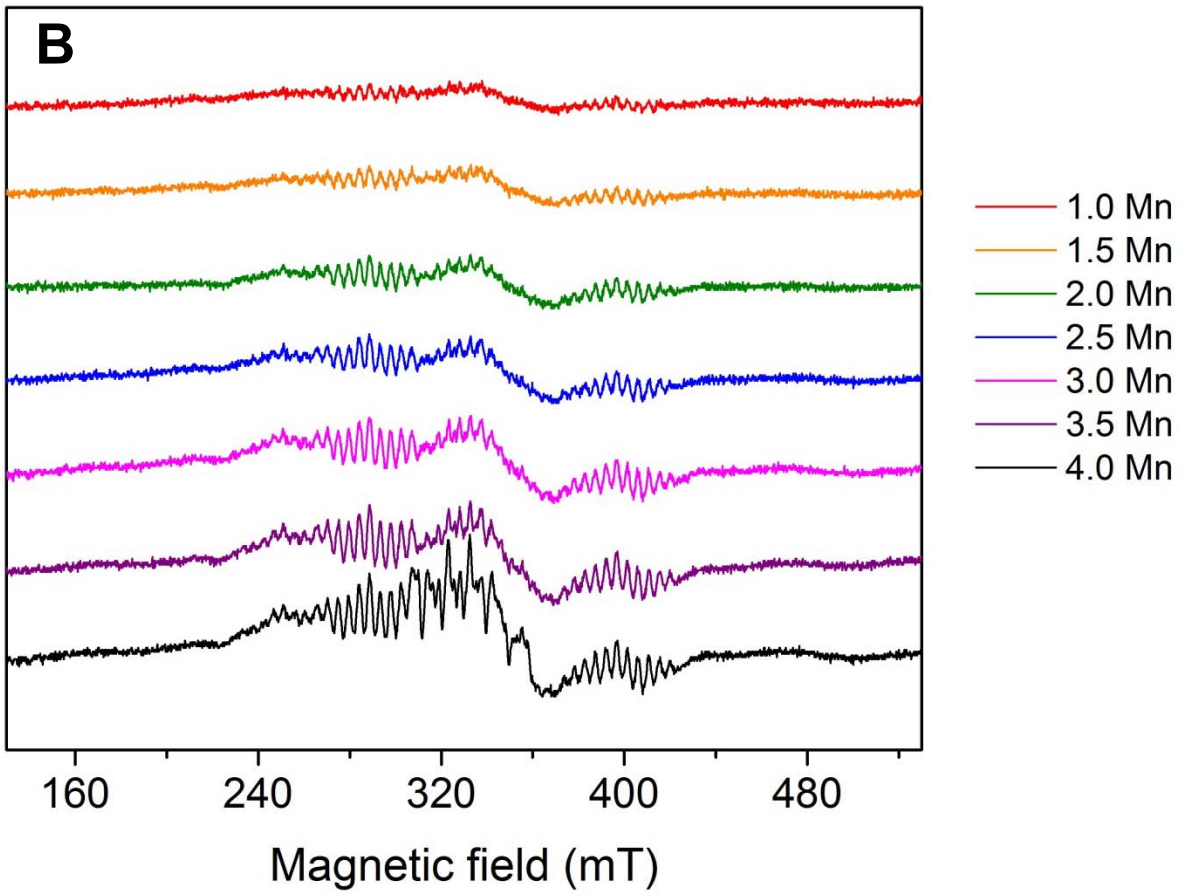

Figure S4. Variable temperature CW EPR spectra of the Mn^{II}_2 form of NrdF. Spectra were acquired at 4.85, 7.50, 10.0, 12.5, 17.0, 25.0, 40.0, 60.0, 80.0, 100, and 120 K. The spectrometer settings were: microwave frequency = 9.38 GHz; power = 50 μW; modulation amplitude = 0.5 mT; modulation frequency = 100 kHz; sweep rate = 5.3 mT/s. Inset: the double integral of EPR intensity from 0−700 mT as a function of temperature, indicating antiferromagnetic coupling of the Mn^{II} ions.

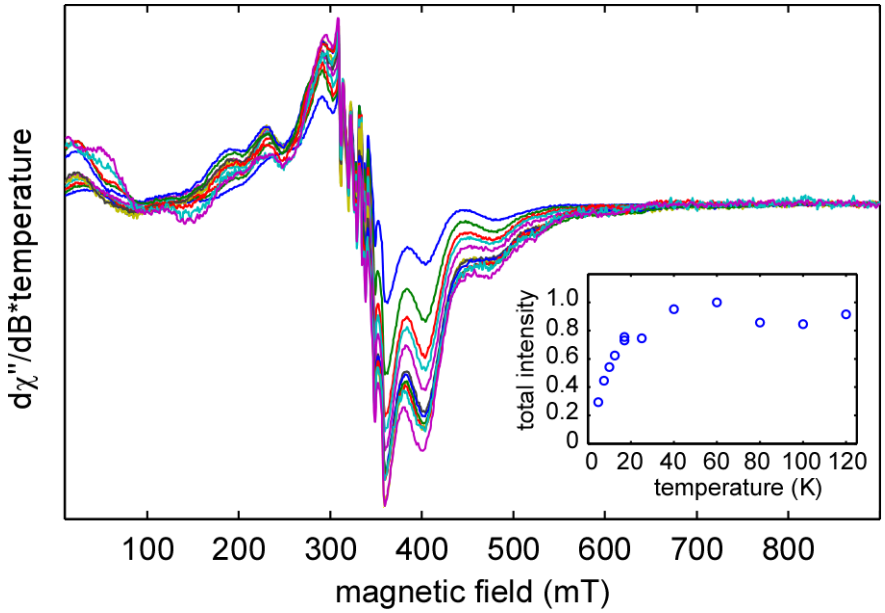

Figure S5. Variable temperature CW EPR spectra of assembled Mn^{III}_2-Y• cofactor of NrdF. The intensity for each of the bottom four spectra in the series was scaled by the noted percentage to facilitate comparison. Spectrometer settings: microwave frequency = 9.39 GHz; modulation amplitude = 0.1 mT; modulation frequency = 100 kHz; sweep rate = 0.6 mT/s. Inset: comparison of the 100 K spectrum (black trace) with a simulation (gray trace) obtained using parameters given in the Supporting Information and discussed in the text. The asterisk indicates a contribution to the spectrum from quartz radical.

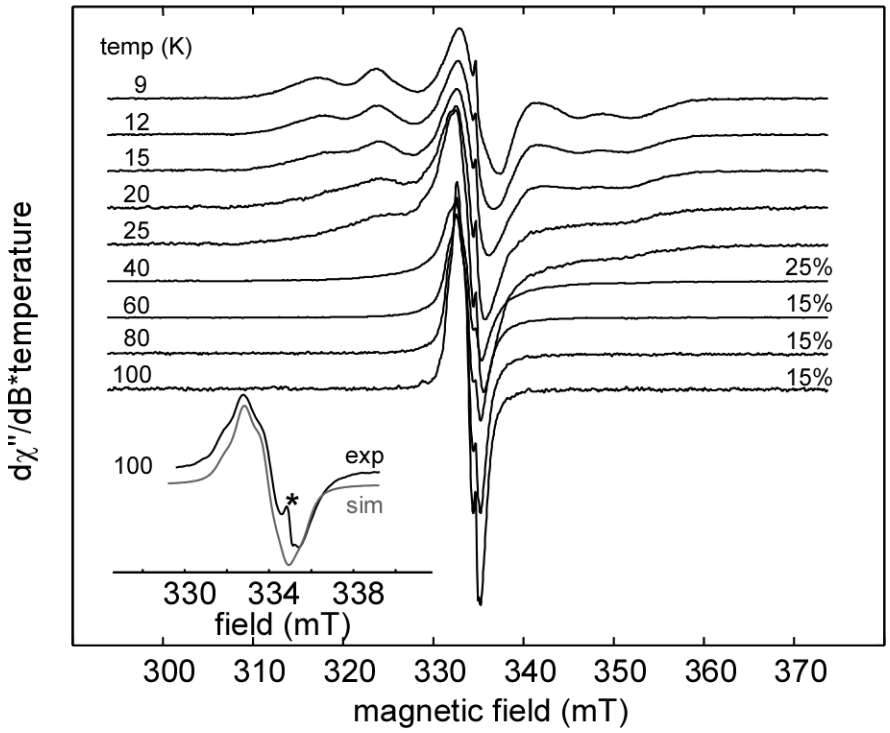

Figure S6. Effect of the β-proton dihedral angle (Θ) on the simulated EPR spectrum of Y•. The experimental spectrum is the same as that from the inset of Figure S5.

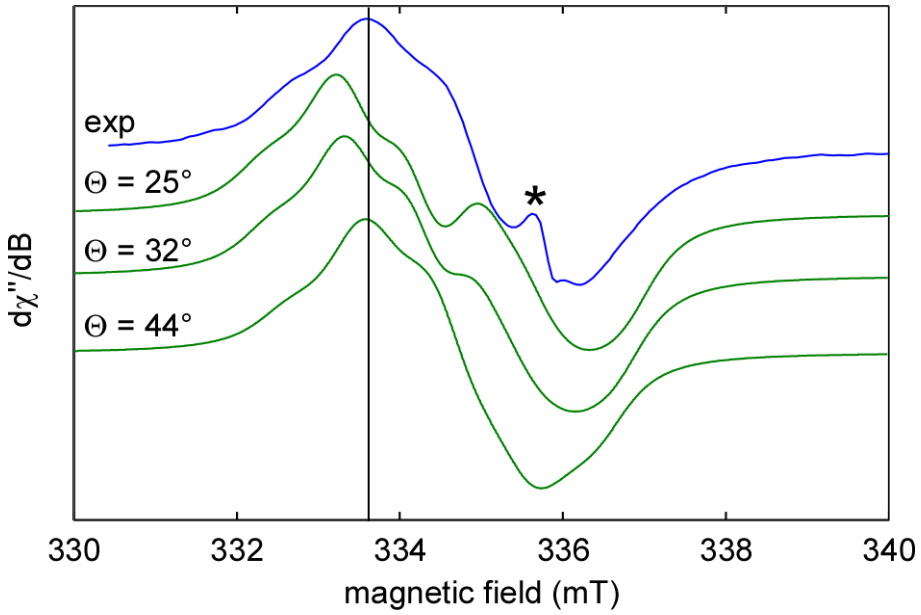

Figure S7. Binding of *B. subtilis* $NrdI_{hq}$ to Mn^{II}-loaded NrdF monitored by spectrofluorometry. (A) Fluorescence emission spectra (λ_{ex} = 380 nm) of 2 μM $NrdI_{hq}$ alone (black) and in the presence of 15 μM (red) and 25 μM (blue) Mn^{II}-loaded NrdF (4 Mn^{II}/β2). From the relative fluorescence at the emission maximum of 517 nm, the ratio of the molar fluorescence of bound and unbound $NrdI_{hq}$ was 2.4. (B) Analysis of a typical titration to determine the K_d for $NrdI_{hq}$ binding to Mn^{II}-loaded NrdF. The cuvette (700 μL) contained 1 μM apoNrdF, 4 Mn^{II}/β2, and 100 μM dithionite in Buffer B, into which was titrated a solution of 240 μM $NrdI_{hq}$ and 100 μM dithionite in Buffer B. The plot shown is of fluorescence change attributed to $NrdI_{hq}$ binding (ΔF) vs. free $NrdI_{hq}$ concentration, extracted from the data from this titration according to section S1.1. The data are fit to equation S4 (red). For this particular titration, K_d = 0.4 ± 0.1 μM and n = 1.7 ± 0.1. The results from four titrations were averaged to yield the values of K_d = 0.6 ± 0.2 μM and n = 1.6 ± 0.1 given in the main text.

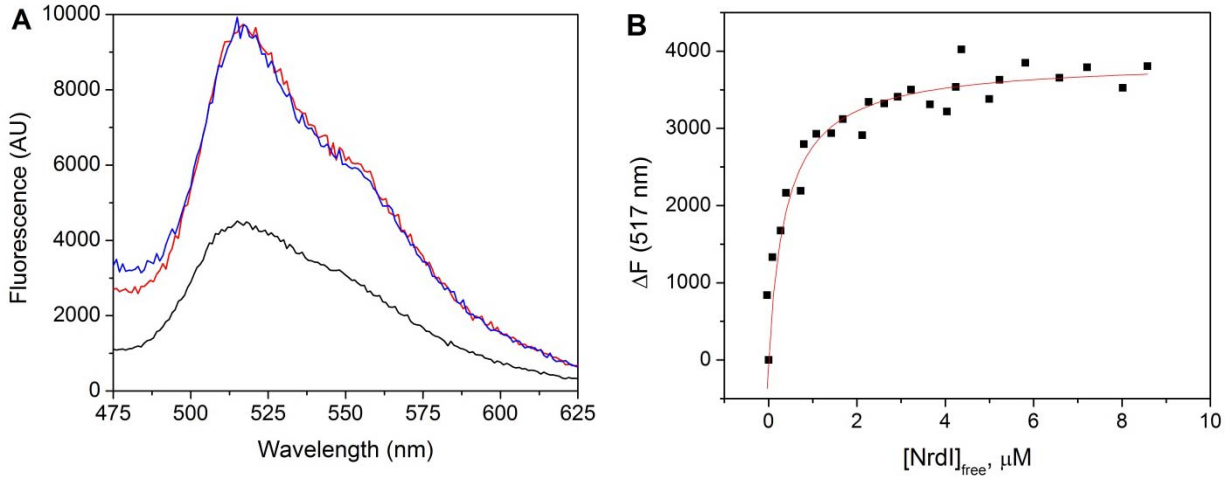

Figure S8. Comparison of the A_{610} traces of reaction of $NrdI_{hq}$ with O_2 in the presence and absence of SOD at 25 °C. (A) $NrdI_{hq}$ (20 μM), mixed 1:1 with O_2-saturated buffer and 0 (blue) or 500 (black) U/mL SOD. The data are fit to two exponentials: 3.4 and 1.1 s^{-1} (without SOD), and 1.7 and 1.1 s^{-1} (with SOD). Similar results were obtained using 100 U/mL SOD. (B) $NrdI_{hq}$ (20 μM), mixed 1:1 with O_2-saturated buffer, Mn^{II}-loaded NrdF (50 μM, 3.5 Mn^{II}/β2), and 0 (black) or 500 (red) U/mL SOD. There is not a significant difference between the kinetics of reactions carried out without SOD versus with 50 U/mL SOD (after mixing), as long as Mn^{II}-loaded NrdF is present (not shown).

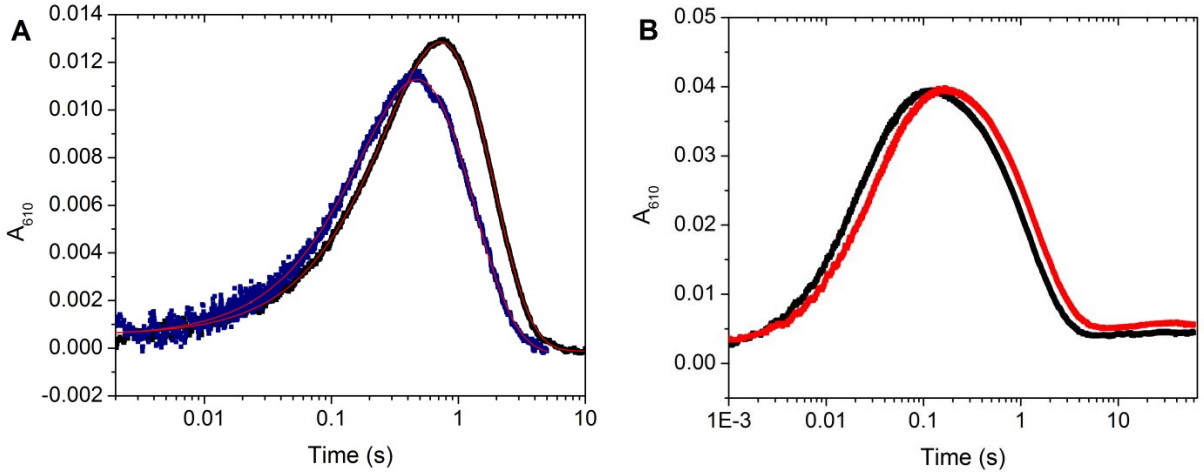

Figure S9. Reaction of $NrdI_{hq}$ with O_2 in the presence of SOD at 25 °C, monitored by SF UV-vis $NrdI_{hq}$ (20 μM) in Buffer B was mixed 1:1 with O_2-saturated buffer containing SOD (500 U/mL). Kinetic traces (2000 points, 0-10 s) were acquired every 10 nm between 310 and 700 nm. A) Point-by-point reconstructions of the reaction spectra for a representative experiment at the indicated timepoints. B) Spectra of $NrdI_{ox}$, $NrdI_{sq}$, and $NrdI_{hq}$, extracted from global analysis of the multiwavelength data in KinTek Explorer with SpectraFit, fitted to eq. 1, 2, and 4 in the main text (section 3.5). These fits yielded k_1 = 1.4 ± 0.3 s^{-1} and k_2 = 1.5 ± 0.4 s^{-1} (five independent experiments). Including $k_{\pm 4}$ did not significantly affect goodness of fit or the rate constants. Although the residuals (C) were good, the extracted spectrum of $NrdI_{sq}$ was not the same as in Figure 1A, with extinction coefficients ~1 mM^{-1} cm^{-1} higher in the 450-500 nm region and ~1 mM^{-1} cm^{-1} lower in the 550-650 nm region, suggesting a contribution of $NrdI_{ox}$ to the extracted $NrdI_{sq}$ spectrum. C) Residuals for the fit at each timepoint listed in A. Each residual trace is offset by 0.001, represented by a tick.

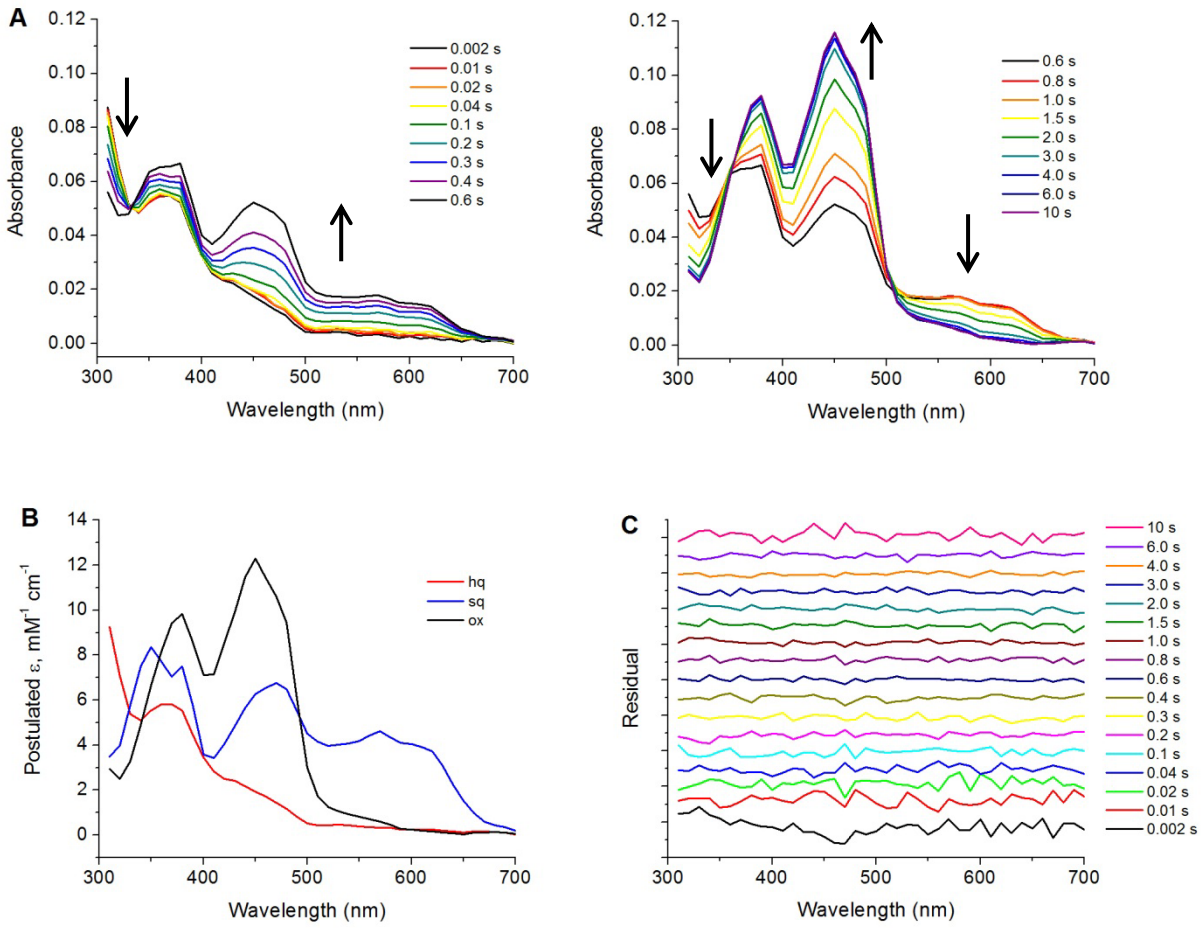

Figure S9, continued. D) Spectra of $NrdI_{ox}$, $NrdI_{sq}$, and $NrdI_{hq}$, extracted from global analysis of the multiwavelength data in KinTek Explorer with SpectraFit, fitted to eq. 1-4 in the main text (see section 3.5). E) Residuals for the fit at each timepoint listed in A. Each residual trace is offset by 0.001, represented by a tick.

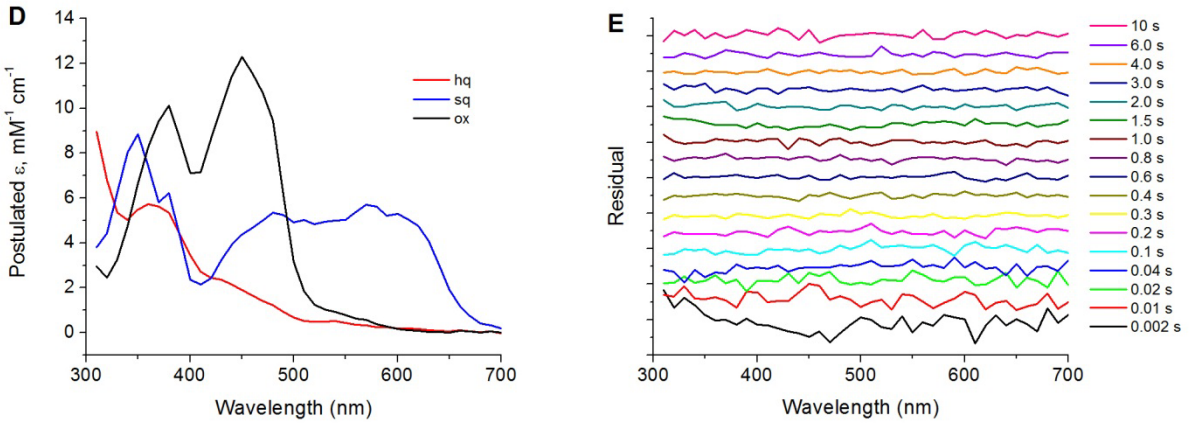

Figure S10. Reaction of $NrdI_{hq}$ with O_2 in the presence of SOD, in the absence (A) and presence (B) of apoNrdF. $NrdI_{hq}$ (20 μM) was mixed 1:1 with O_2-saturated buffer containing 500 U/mL SOD, 25 °C, monitored at 610 nm. In (B), the O_2-saturated buffer syringe also contained 50 μM apoNrdF. (A) The data, the average of five independent experiments, were fit to two exponentials. The rate constants are shown in Table 1: 1.6 s^{-1} and 1.1 s^{-1}. (B) The data from five experiments were fit to three exponentials. The rate constants are shown in Table 1: 18 s^{-1} (ΔA = 0.009), 7.4 s^{-1} (ΔA = 0.026), and 0.93 s^{-1} (ΔA = -0.035). Residuals are shown at the bottom of the plot. The data were fit and plotted in Origin.

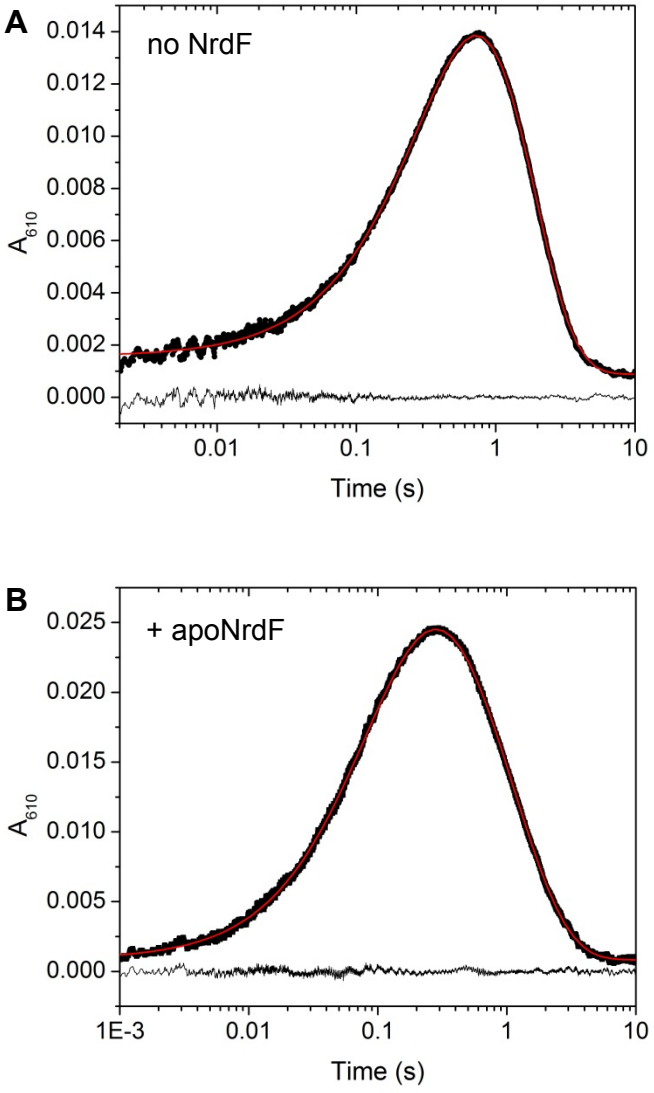

Figure S11. Rates of NrdI comproportionation and disproportionation monitored by SF UV-visible spectroscopy. The contents of syringes containing anaerobic solutions of 20 μM $NrdI_{hq}$ and 20 μM $NrdI_{ox}$ (with or without 80 μM apoNrdF) were mixed 1:1 and A_{610} was monitored. A) The reaction in the absence of NrdF. B) The reaction in the presence of 40 μM apoNrdF (after mixing). The plots were fit to eq. 4 in the main text (red line), using KinTek Explorer. Residuals are shown at the bottom. For these traces, k_{+4} = 17 mM^{-1} s^{-1} and k_{-4} = 21 mM^{-1} s^{-1} (A), and k_{+4} = 0.8 mM^{-1} s^{-1} and k_{-4} = 1.2 mM^{-1} s^{-1} (B).

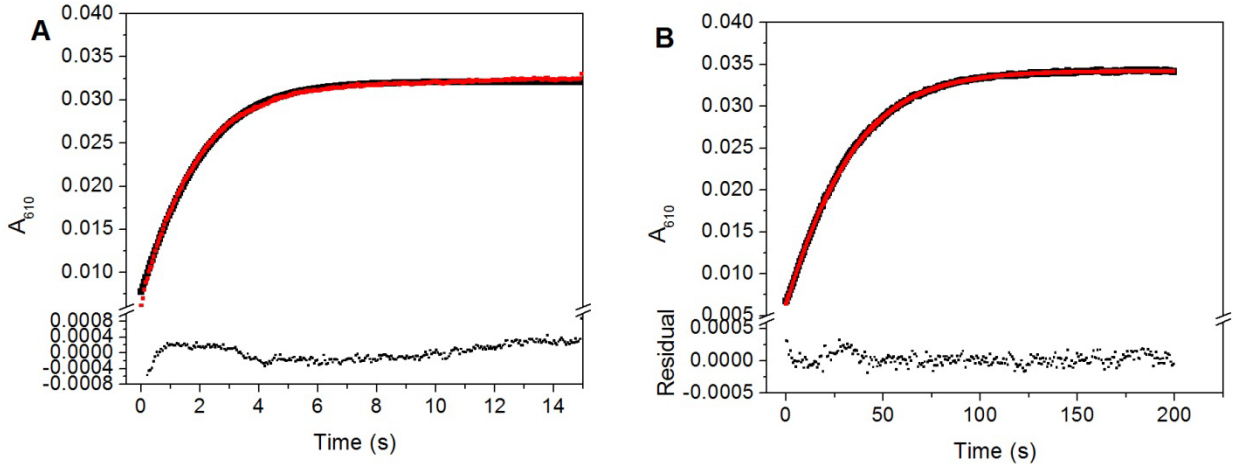

Figure S12. Representative single wavelength SF traces for the reaction of $NrdI_{hq}$ with O_2 in the presence of Mn^{II}-loaded NrdF at 25 °C. $NrdI_{hq}$ (100 μM) and Mn^{II}-loaded NrdF (150 μM, 3.5 $Mn^{II}/\beta 2$) were mixed 1:1 with O_2-saturated buffer. Fits are in red and residuals are shown at the bottom of each plot. (A) 610 nm, fit to four exponentials. (B) 340 nm, fit to four exponentials. (C) 410 nm, fit to three exponentials. The data were fit and plotted in Origin. Rate constants for the fits are shown in Tables 2, 3, and S3.

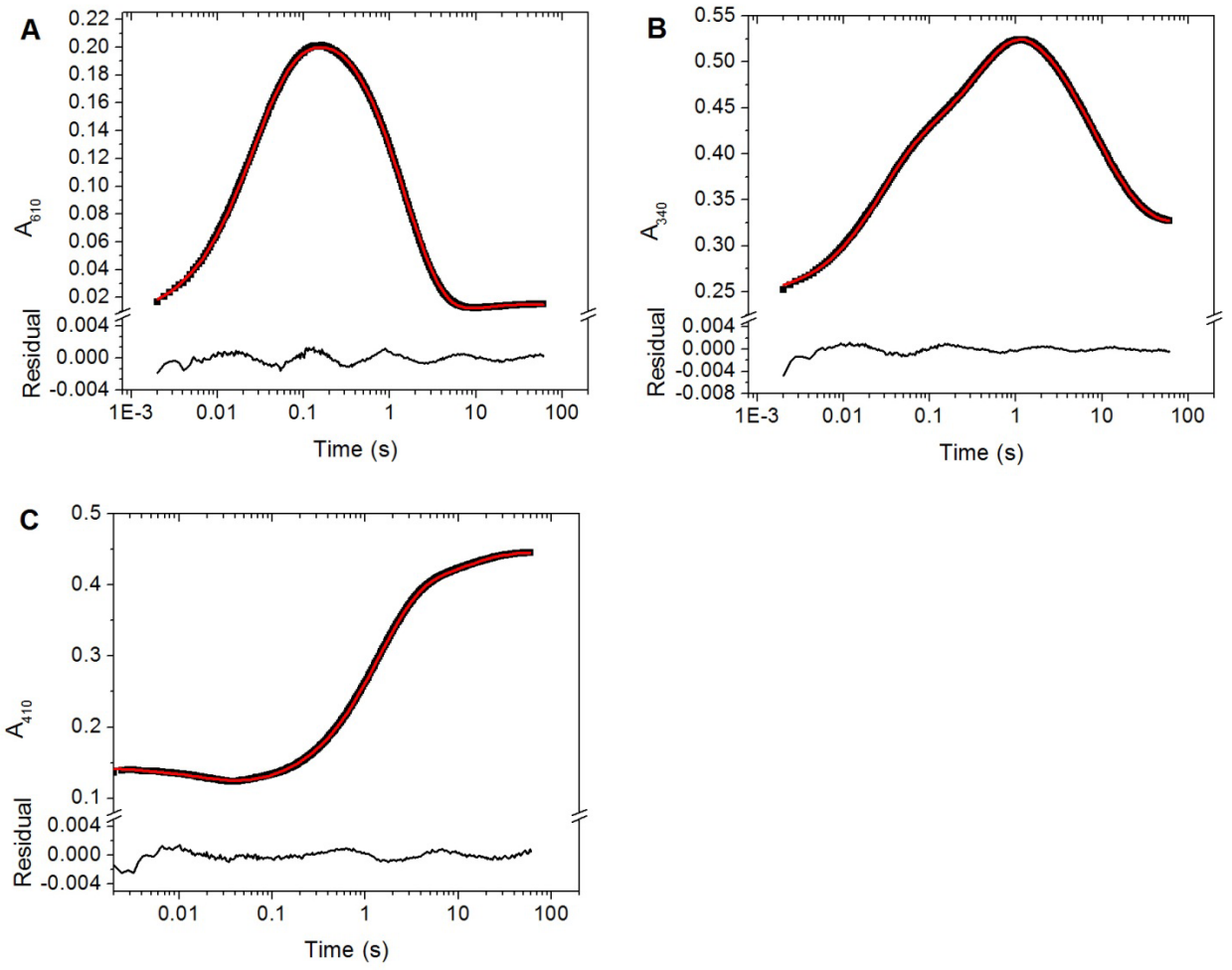

Figure S13. O_2 dependence of apparent rate constants for reaction of 20 μM $NrdI_{hq}$ mixed 1:1 with 25%, 50%, 75%, and 100% O_2-saturated buffer (~0.3, 0.6, 0.9, and 1.3 mM O_2 before mixing, as shown on x-axis) containing 50 μM Mn^{II}-loaded NrdF (3.5 Mn^{II}/β2). Data were collected at 340, 410, and 610 nm (at least 4 traces at each wavelength), in two independent sets of experiments, and fit to 4 exponentials (340 and 610 nm) or 3 exponentials (410 nm) as described in the main text. For the phases shown in (A)-(D), data were not included if a given phase was not observed at a given wavelength (e.g. for sq formation phase 2 at 410 nm in B, or for $Mn^{III}Mn^{IV}$ decay/Y• formation at 610 nm in D), or if the phase's amplitude is very small (e.g. 410 nm in A).

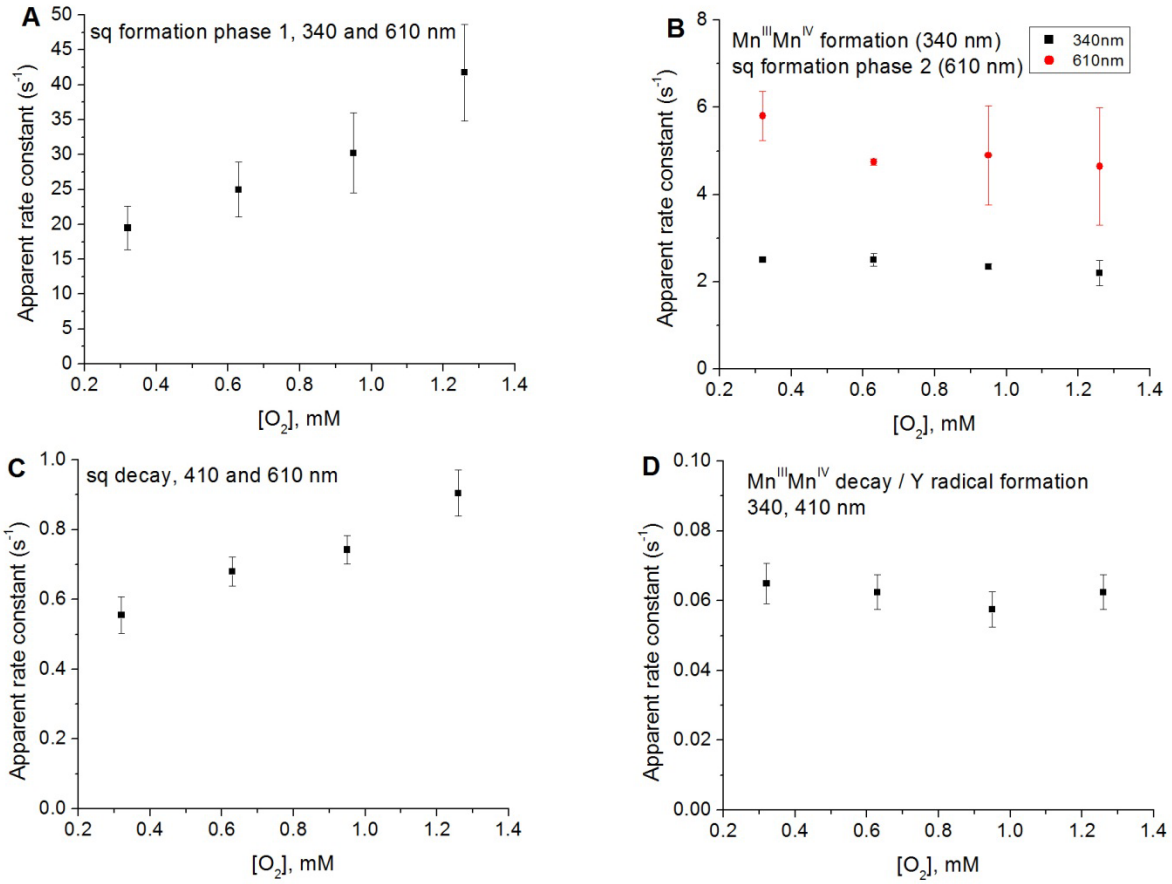

Figure S14. Estimated UV-vis spectrum of the putative $Mn^{III}Mn^{IV}$ intermediate, determined as described in the main text.

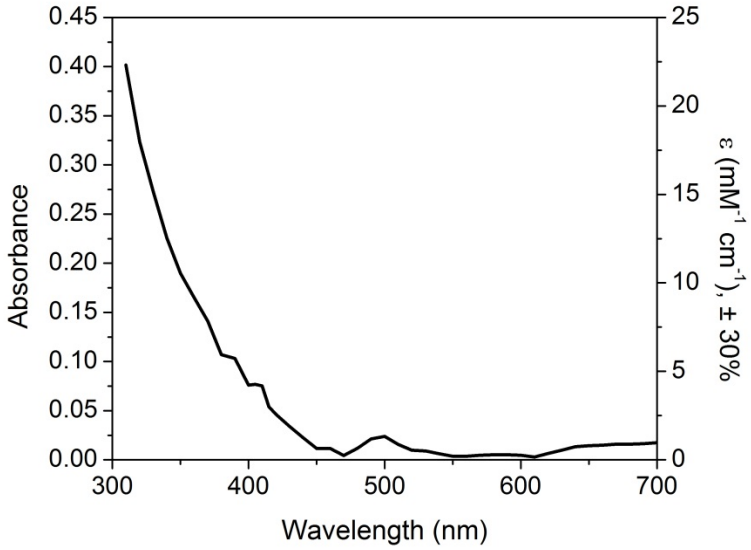

Figure S15. Overlay of EPR spectra (A) for a representative RFQ time course in the reaction of Mn^{II}_2-NrdF•$NrdI_{hq}$ with O_2. (B) Comparison of spectra to illustrate a small but significant shift from 270.1 (indicated at right) to 271.3 mT in the lowest-field line from the 12 ms to 535 ms samples, which suggests some heterogeneity (e.g. more than one protonation state) of the intermediate. Shifts are also observed in other hyperfine peaks. Note also the different relative intensities with time of the features indicated with red arrows. Acquisition parameters: 10 K, 0.1 mW, 9.385 GHz, 100 kHz modulation frequency, 0.4 mT modulation amplitude, 2.52×10^4 gain, 5.12 ms time constant.

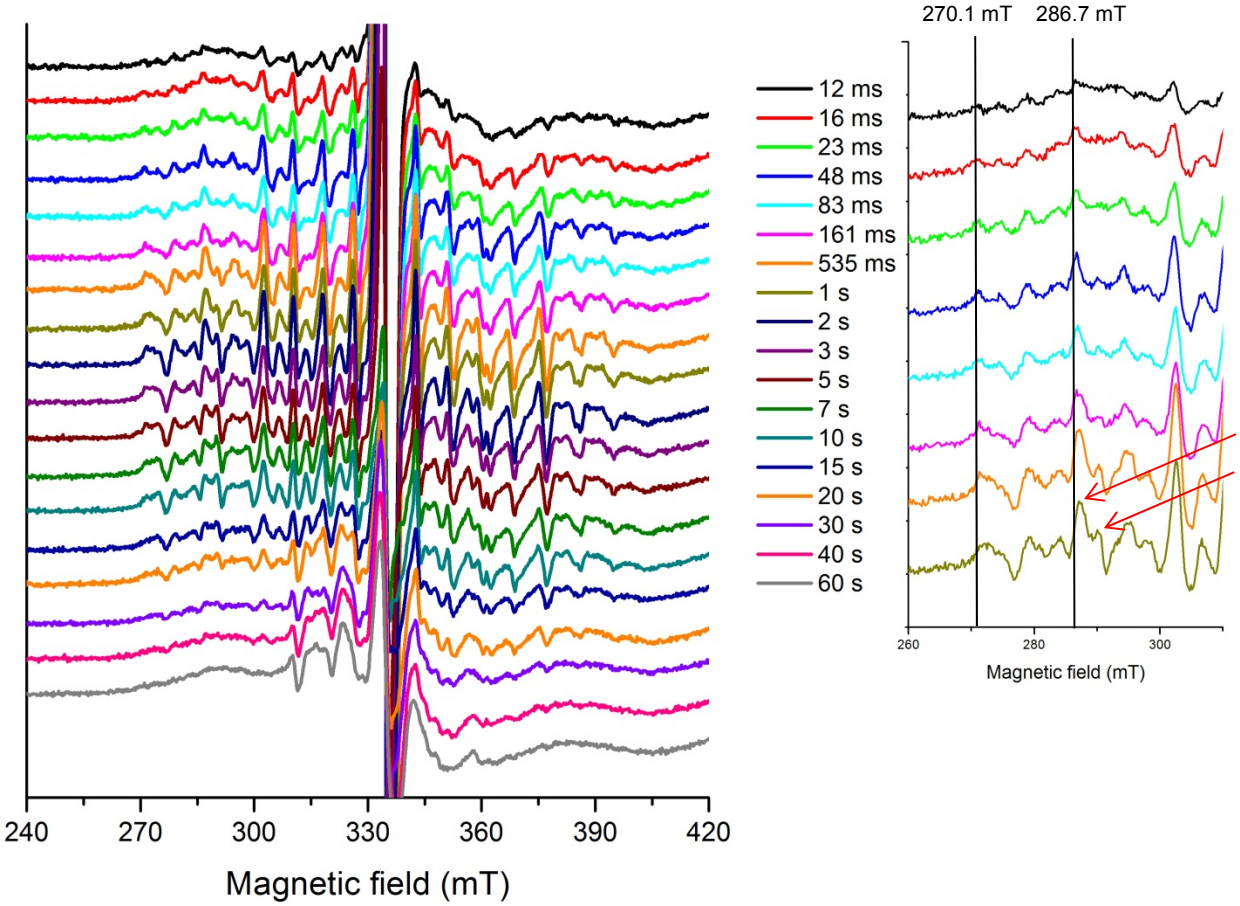

Figure S16. Concentration of the $Mn^{III}Mn^{IV}$ intermediate, determined by scaling the relative concentrations (Figure 7, main text) according to a factor obtained from simulation and spin quantification of three RFQ samples as described in Figure 6. The data (black, mean ± SD for 2-4 independent experiments) are fitted to a two phase model (red) with rate constants given in Table 3.

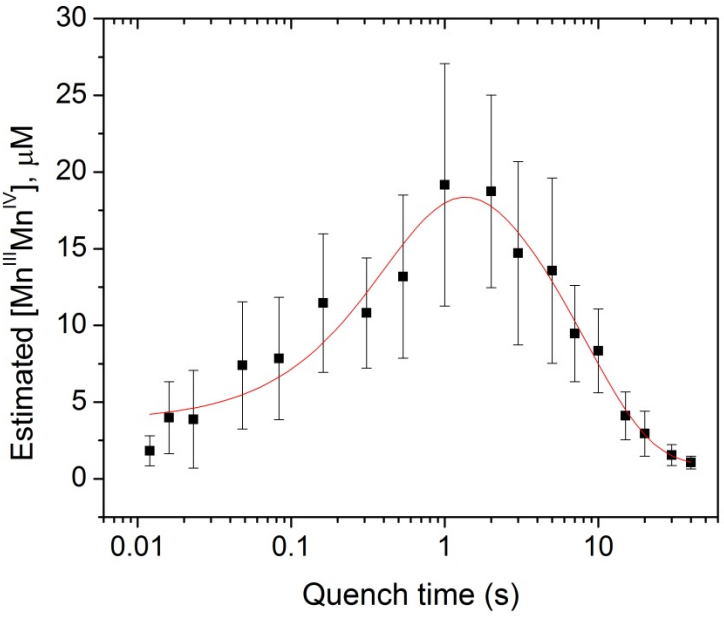

Figure S17. Characterization of Y105F NrdF. (A) SDS-PAGE (12.5%) analysis of 3 μg apo-Y105F NrdF (lane 2). Molecular weight markers (kDa) are shown in lane 1. (B) EPR spectrum (10 K) of 75 μM apo-Y105F NrdF, incubated with 3.5 Mn^{II}/β2. Acquisition parameters: 9.385 GHz, 0.1 mW power, 0.4 mT modulation amplitude, 100 kHz modulation frequency, 2.52×10^4 gain, 5.12 ms time constant.

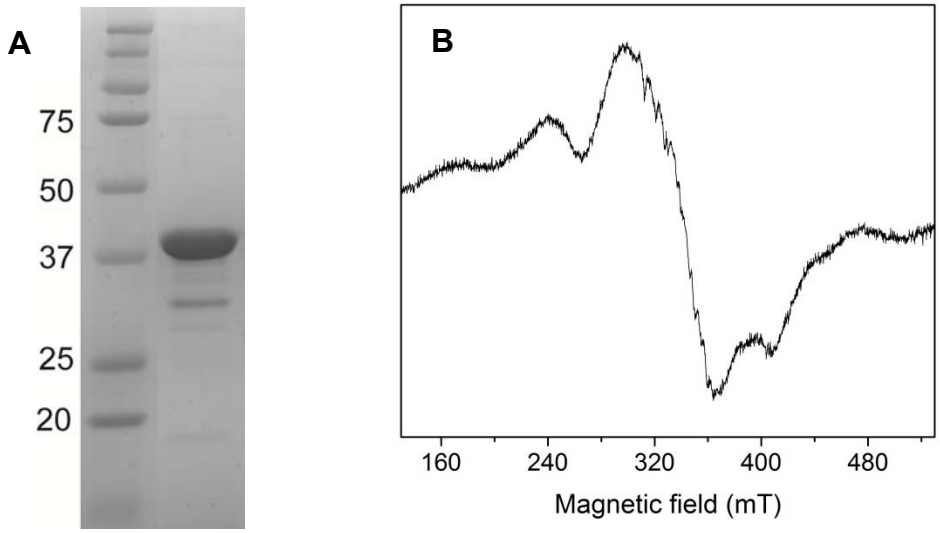

Figure S18. Fluorescence titration of $NrdI_{hq}$ with Mn^{II}_2-Y105F-NrdF. The cuvette contained 700 μL 5 μM $NrdI_{hq}$ in Buffer B, into which 150 or 200 μM Mn^{II}-loaded Y105F NrdF (4 Mn^{II}/β2) was titrated. The percent increase in fluorescence at 517 nm against μM Y105F NrdF added is plotted for two experiments. For comparison, the maximum fluorescence increase for a titration of $NrdI_{hq}$ with wt Mn^{II}_2-NrdF was 140%. Given that saturation was not observed under these conditions, we cannot rule out that $NrdI_{hq}$ binds to Mn^{II}_2-Y105F-NrdF incorrectly (with a lower fluorescence change upon binding) with a lower K_d.

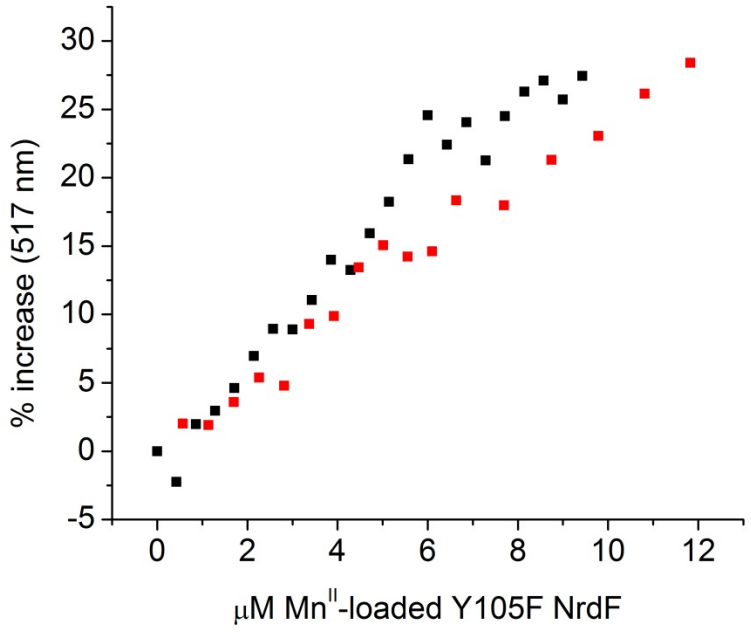

Figure S19. Reaction of $NrdI_{hq}$ (20 μM) mixed 1:1 with O_2-saturated buffer containing Mn^{II}-loaded NrdF-Y105F (50 μM NrdF, 3.5 Mn/β2) and SOD (500 U/mL), at 25 °C, monitored by SF absorption spectroscopy. Kinetic traces (2000 points, 0-10 s) were acquired every 10 nm between 310 and 700 nm and point-by-point reconstructions of the reaction spectra are shown for a representative experiment at the indicated timepoints. The results demonstrate a slight acceleration of the k_{app} for sq formation (5.4 s^{-1}) relative to $NrdI_{hq}$ in the absence of NrdF, but 10-fold less than Mn^{II}-loaded wt NrdF. No features suggestive of the $Mn^{III}Mn^{IV}$ are apparent (compare with Figure 4).

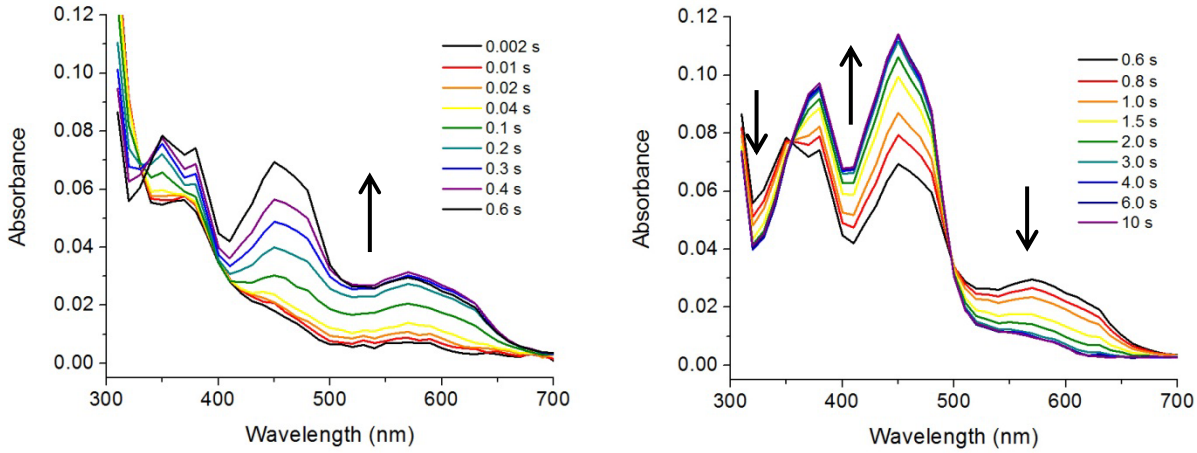

Figure S20. Proposal that the conformational change suggested to rate limit $Mn^{III}Mn^{IV}$ intermediate formation during Mn^{III}_2-Y• cofactor assembly is a reorganization of the αE helix of NrdF. The difference in structure of the αE helical region between E158 and Y163 (*E. coli* numbering) between reduced and oxidized NrdF was first noted by Eklund and coworkers for the diferrous and diferric forms of *S.* Typhimurium NrdF,[32] but this comparison holds for dimanganese forms of NrdF crystallized to date as well.

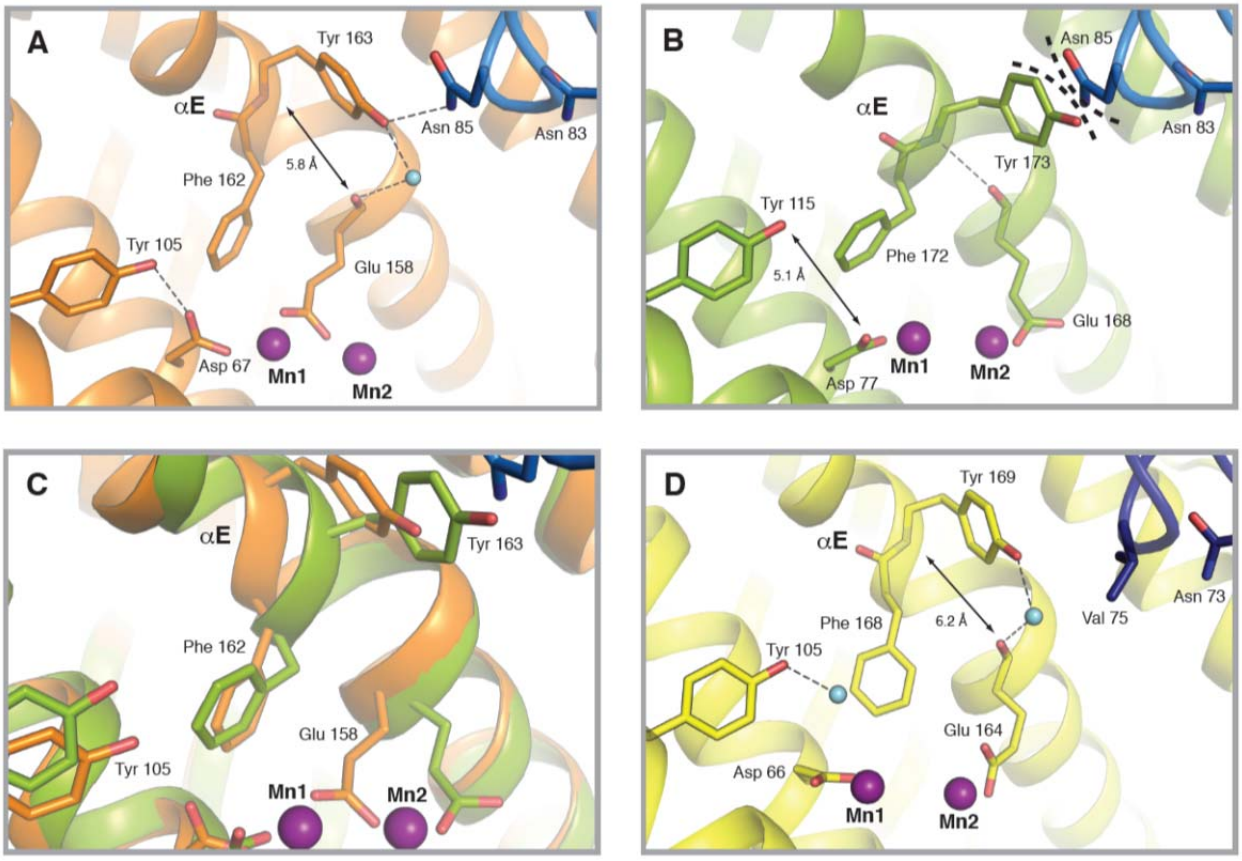

(A) The *E. coli* Mn^{II}_2-NrdF•$NrdI_{hq}$ complex.[25] NrdF is in orange and NrdI is in blue. The residues shown in sticks are completely or nearly completely conserved in class Ib RNRs. Dashed lines indicate hydrogen bonds. Note the hydrogen bonds between Y163 of NrdF and N85 of NrdI and between Y163 and E158, mediated by a solvent molecule (light blue) in the oxidant channel. (B) *C. ammoniagenes* Mn^{III}_2-NrdF. When the metal site is oxidized, the hydrogen bond between Y115 and D77 present in (A) is disrupted, and the αE helix compresses to allow for the backbone CO of E168 to hydrogen bond to the amide NH of Y173. In this configuration, Y173 sterically clashes with N85 of NrdI (using the *E. coli* Mn^{II}_2-NrdF/$NrdI_{hq}$ complex as a model). Thus this helical movement, connecting the metal site, channel, and NrdI binding site, could serve as a mechanism to cause dissociation of NrdI once $O_2^{\bullet-}$ reaches the metal site. (C) Overlay of (A) and (B), emphasizing the shift in the αE helix, residues D67, Y105, F162, and Y163 (all *E. coli* numbering), that accompanies oxidation of the metal site. (D) Model of the *B. subtilis* Mn^{II}_2-NrdF/$NrdI_{hq}$ complex, based on the individual structures of *B. subtilis* NrdI and Mn^{II}_2-NrdF and *E. coli* Mn^{II}_2-NrdF/$NrdI_{hq}$.[33] First, note the similar αE conformation to that in (A). No *B. subtilis* Mn^{III}_2-NrdF structure is available for comparison

with (B). Note also that a solvent molecule is hydrogen bonded to Y105 (as well as to E198, not shown, a ligand to both Mn1 and Mn2). It is possible that in the Y105F mutant this solvent molecule is absent, which could allow F168 to adopt a conformation as in (B) to compensate. This, in turn, could result in a similar αE helical movement to extrude Y169. Although *B. subtilis* is part of a small number of class Ib systems whose NrdI contains a V at the position of *E. coli* N85, the displacement of Y169 would also sterically clash with V75 and disrupt $NrdI_{hq}$ binding. An associated loss of the light blue solvent molecule in the channel could also disrupt oxidant channeling.

S4. SUPPLEMENTARY REFERENCES

(1) Eftink, M. R. *Methods Enzymol.* **1997**, *278*, 221-257.

(2) The Mn cluster contributes ~6 mM^{-1} cm^{-1} to the ε at this wavelength, as determined by incubation of 10 μM Mn^{III}_2-Y• NrdF with 1 mM NH_2OH until no further change was observed, 25 min. This minor contribution was ignored.

(3) Geiger, R. A.; Chattopadhyay, S.; Day, V. W.; Jackson, T. A. *J. Am. Chem. Soc.* **2010**, *132*, 2821-2831.

(4) Petersson, L.; Graslund, A.; Ehrenberg, A.; Sjoberg, B. M.; Reichard, P. *J. Biol. Chem.* **1980**, *255*, 6706-12.

(5) Zhang, Y.; Stubbe, J. *Biochemistry* **2011**, *50*, 5615-5623.

(6) Bull, C.; Fee, J. A. *J. Am. Chem. Soc.* **1985**, *107*, 3295-3304.

(7) Valentine, J. S.; Curtis, A. B. *J. Am. Chem. Soc.* **1975**, *97*, 224-226.

(8) Massey, V.; Palmer, G. *Biochemistry* **1966**, *5*, 3181-3189.

(9) Palmer, G.; Müller, F.; Massey, V. In *Flavins and Flavoproteins: Proceedings of the Third International Symposium on Flavins and Flavoproteins*; Kamin, H., Ed.; University Press: Baltimore, 1971, p 123-140.

(10) Tomter, A. B.; Zoppellaro, G.; Andersen, N. H.; Hersleth, H.-P.; Hammerstad, M.; Røhr, Å. K.; Sandvik, G. K.; Strand, K. R.; Nilsson, G. E.; Bell, C. B., III; Barra, A.-L.; Blasco, E.; LePape, L.; Solomon, E. I.; Andersson, K. K. *Coord. Chem. Rev.* **2013**, *257*, 3-26.

(11) Brynda, M.; Britt, R. D. *Res. Chem. Intermed.* **2007**, *33*, 863-883.

(12) Fessenden, R. W.; Schuler, R. H. *J. Chem. Phys.* **1963**, *39*, 2147-2195.

(13) Svistunenko, D. A.; Cooper, C. E. *Biophys. J.* **2004**, *87*, 582-595.

(14) Boal, A. K.; Cotruvo, J. A., Jr.; Stubbe, J.; Rosenzweig, A. C. *Biochemistry* **2012**, *51*, 3861-3871.

(15) Mayhew, S. G.; Ludwig, M. L. In *The Enzymes*; Boyer, P. D., Ed.; Academic Press, Inc.: New York, 1975; Vol. XII, p 57-118.

(16) Massey, V.; *J. Biol. Chem.* **1994**, *269*, 22459-22462.

(17) Eberlein, G.; Bruice, T. C. *J. Am. Chem. Soc.* **1982**, *104*, 1449-1452.

(18) Bruice, T. C. *Isr. J. Chem.* **1984**, *24*, 54-61.

(19) Ballou, D. P. Ph.D. Thesis, University of Michigan, 1971.

(20) Sucharitakul, J.; Prongjit, M.; Haltrich, D.; Chaiyen, P. *Biochemistry* **2008**, *47*, 8485-8490.

(21) Pennati, A.; Gadda, G. *Biochemistry* **2011**, *50*, 1-3.

(22) The contribution from the reaction in eq. 4 can be ignored for normal flavodoxins.

(23) Ballou, D. P.; Entsch, B.; Cole, L. J. *Biochem. Biophys. Res. Commun.* **2005**, *338*, 590-598.

(24) Experiments were also carried out at 10 μM and 40 μM, with similar results.

(25) Boal, A. K.; Cotruvo, J. A., Jr.; Stubbe, J.; Rosenzweig, A. C. *Science* **2010**, *329*, 1526-1530.

(26) Jung, J.; Tollin, G. *Biochemistry* **1981**, *20*, 5124-5131.

(27) Bollinger, J. M., Jr.; Edmondson, D. E.; Huynh, B. H.; Filley, J.; Norton, J. R.; Stubbe, J. *Science* **1991**, *253*, 292-298.

(28) Tong, W.; Burdi, D.; Riggs-Gelasco, P.; Chen, S.; Edmondson, D.; Huynh, B. H.; Stubbe, J.; Han, S.; Arvai, A.; Tainer, J. *Biochemistry* **1998**, *37*, 5840-5848.

(29) Yun, D.; Krebs, C.; Gupta, G. P.; Iwig, D. F.; Huynh, B. H.; Bollinger, J. M., Jr. *Biochemistry* **2002**, *41*, 981-90.

(30) Cotruvo, J. A., Jr.; Stubbe, J. *Biochemistry* **2010**, *49*, 1297-1309.

(31) Bielski, B. H. J.; Allen, A. O. *J. Phys. Chem.* **1977**, *81*, 1048-1050.

(32) Eriksson, M.; Jordan, A.; Eklund, H. *Biochemistry* **1998**, *37*, 13359-13369.

(33) Boal, A. K.; Cotruvo, J. A., Jr.; Stubbe, J.; Rosenzweig, A. C. *Biochemistry* **2012**, *51*, 3861-3871.